Progress In Electromagnetics Research M, Vol. 6, 75–90, 2009

THE CYCLE SLIPPING PHENOMENON AND THE DEGENERATION EFFECT OF GUIDED-WAVE MODES

L. A. Pazynin

Department of Mathematical Physics
Usikov Institute for Radiophysics and Electronics
12, Ac. Proskura St., Kharkov 61085, Ukraine

Abstract—A model of the ring waveguide of a fixed cross-section and variable distribution of the surface impedance of waveguide's wall has been considered. For a class of circular hodographs of surface impedance the analytical solution of the corresponding boundary-value problem has been obtained. This solution has been used for simulating a 'cycle slipping' phenomenon, known from the observations of VLF signals propagating over long paths in the earth-ionosphere waveguide, with the goal of clarifying the cause for its initiation. Numerical experiments have shown that this phenomenon, in the context of the model in question, is a consequence of the interconversion of two dominant waveguide modes in circumstances where their propagation constants are close.

1. INTRODUCTION

Electromagnetic VLF propagation in the earth-ionosphere waveguide has been studied intensively in the last four decades [1–4]. In particular, the analysis of peculiarities of the wave processes in this range is of importance in developing global navigation systems. One feature of this kind has been revealed in experimental observations of diurnal variations of VLF signals over long paths [5] what is known as *'cycle slipping'* (CS) lying in the fact that the initial and final phase values differ by $\pm 2\pi m$ (as a rule, $m = 1$) in diurnal phase records. The CS phenomenon corresponds to an extremely deep fading of the received signal. This phenomenon can be explained in a qualitative sense starting from the assumption [6] that not only the principal (first) mode arrives at the observation point but also do the second mode and the higher-order modes resulting from the transformation of

the principal mode on a waveguide discontinuity at the intersection of the path and the terminator (i.e., the sunrise or sunset line).

With the aim of numerical simulation of the above-mentioned phenomenon, different modifications of irregular waveguides have been investigated. In particular, in papers [7, 8], the first-into-second-mode conversion coefficient has been calculated by the method of partial domains for a number of two-dimensional impedance waveguides. In the approximation taking no account of the reflection from a discontinuity, its magnitude did not exceed 0.5 even for an abrupt stepwise change of the waveguide height. For the same purpose, the method of cross-sections [9] developed for wave guiding structures with slowly varying parameters over a wavelength has been used in [10]. A two-dimensional model represented a coaxial waveguide with varying in azimuth cross-section and surface impedance Z of one wall. The above-mentioned conversion coefficient reached 1.2, what, as the authors noted, was also too small to explain the CS phenomenon occurring mostly away from the terminator. The approach developed in [8] has been extended in a number of papers to a case of the waveguide whose upper wall is a flat-layered anisotropic medium [11].

The results of all these investigations cast doubt on the statement that the CS phenomenon can be explained purely by the diffraction effect of the conversion of the principal mode into the higher-order modes during its scattering on the section of variable cross-section of a waveguide. In regular waveguides whose walls are of finite conductivity being constant along the structure, the more efficient mode-interconversion mechanism takes place. It is well known [12] that there exist values of normalized surface impedance of walls $\eta_{i,\,i+1}^{deg}$ such that the propagation constants ν_i and ν_{i+1} of two adjacent (i and $i+1$) waveguide modes coincide. Here $\eta = Z/Z_0$, where $Z_0 = \sqrt{\mu_0/\epsilon_0}$ is the wave resistance of vacuum. In this case the modes together with the associated impedance value are said to be *degenerate*. The mode-interconversion effect occurs in the neighborhood of the degeneracy regime [13]. For example, by varying a complex value of the impedance η of the wall of a regular waveguide such that it describe a closed curve around the degenerate value $\eta_{i,\,i+1}^{deg}$, we get a complete interconversion of i and $i+1$ modes. In particular, the degeneracy of two VLF modes in the natural waveguide has been discussed in [14].

The aim of the present paper is to clear up *the role of the waveguide mode interconversion effect* taking place in the neighborhood of the degeneracy regime *in the occurrence of CS*. In the first part of the work we present a model of the irregular waveguide of a fixed cross-section with varying in azimuth impedance, what is a simplified version of the

model given in [10]. This model allows us to exclude from consideration a diffraction effect of electromagnetic wave transformation on spatial inhomogeneities of walls and to obtain the analytical solution of the associated boundary-value problem for some class of surface impedance distributions. In the second part, with the help of the well-known Watson method, the solution is transformed into a series rapidly converging for large wave sizes of the model. In the third part we present the results of the numerical experiment.

2. STATEMENT AND SOLUTION OF THE PROBLEM

In the cylindrical coordinates ρ, φ, z, consider a azimuthal waveguide formed by a perfectly conducting wall $\rho = a$ and a wall $\rho = b$ with a variable surface impedance (see Fig. 1), in which a filament of a magnetic linear current with the time-dependence $e^{-i\omega t}$ at $\vec{\rho}_0 = \{\rho_0, \varphi_0\}$ generates a TM-polarized field $\vec{E} = i\omega\mu_0\{\partial U/\rho\partial\varphi, -\partial U/\partial\rho, 0\}$, $\vec{H} = k^2\{0, 0, U\}$. The Hertz potential U is the solution of the equation

$$\left(\frac{1}{\rho}\frac{\partial}{\partial\rho}\rho\frac{\partial}{\partial\rho}+\frac{1}{\rho^2}+k^2U(\vec{\rho},\vec{\rho_0})\right) = -\frac{iI^{(m)}}{\omega\rho}\delta(\rho-\rho_0)\delta(\varphi-\varphi_0),$$
$$(a<\rho,\ \rho_0<b,\ -\pi\leq\varphi,\ \varphi_0\leq\pi) \quad (1)$$

with the boundary conditions

$$a)\ \frac{\partial U}{\partial\rho} = 0 \ \text{ for } \ \rho = a; \quad b)\ \frac{\partial U}{\partial\rho} - ik\eta(\varphi)U = 0 \ \text{ for } \ \rho = b, \qquad (2)$$

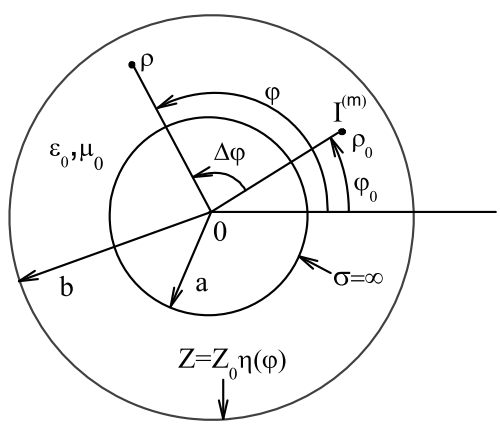

Figure 1. Azimuthal waveguide geometry.

where $k = \omega/c$ is the wave number and $I^{(m)}$ is the linear magnetic current density. Let a normalized surface impedance of the wall $\rho = b$ is given in the form

$$\eta(\varphi) = \eta_0 \frac{e^{i\varphi} + \eta_1}{e^{i\varphi} + \eta_2}, \tag{3}$$

with arbitrary complex parameters η_j ($j = 0, 1, 2$). The values of the function $\eta(\varphi)$ form in the plane of the complex variable η a circle (a hodograph curve) of radius $r_{imp} = |\eta_0(\eta_1 - \eta_2)/(1 - |\eta_2|^2)|$ centered at the point $\eta_{imp} = \eta_0(1 - \eta_1\bar{\eta}_2)/(1 - |\eta_2|^2)$. To find the function U, use the Green's theorem

$$\begin{aligned} &U(\vec{\rho}, \vec{\rho_0}) \\ &= U_0(\vec{\rho}, \vec{\rho_0}) + \int_S \left(U(\vec{\rho_1}, \vec{\rho_0}) \frac{\partial}{\partial N} G(\vec{\rho_1}, \vec{\rho}) - G(\vec{\rho_1}, \vec{\rho}) \frac{\partial}{\partial N} U(\vec{\rho_1}, \vec{\rho}) \right) ds_1, \end{aligned} \tag{4}$$

where N is the outer normal to the boundary S of the ring domain ($a < \rho_1 < b, -\pi < \varphi_1 < \pi$). By choosing as

$$G(\vec{\rho_1}, \vec{\rho}) = -\frac{i}{8} \sum_{n=-\infty}^{\infty} e^{in(\varphi_1 - \varphi)} H_n^{(10)}(ka, k\rho_<) \frac{H_n^{(1)}(k\rho_>)}{H_n^{(1)\prime}(ka)}, \tag{5}$$

the Green function of the space containing the perfectly conducting cylinder of radius a [15], and as the function

$$U_0(\vec{\rho}, \vec{\rho_0}) = -\frac{iI^{(m)}}{k} G(\vec{\rho_0}, \vec{\rho}), \tag{6}$$

the Hertz potential of the field generated by a linear magnetic current in the presence of the conducting cylinder $\rho = a$, we satisfy conditions (1) and a) in (2). In (5), the following notation is used:

$$H_n^{(j_1 j_2)}(x_1, x_2) = \frac{\partial^{j_1}}{\partial x_1^{j_1}} \frac{\partial^{j_2}}{\partial x_2^{j_2}} \left(H_n^{(1)}(x_1) H_n^{(2)}(x_2) - H_n^{(2)}(x_1) H_n^{(1)}(x_2) \right), \tag{7}$$

$j_1, j_2 = 0, 1$; $H_n^{(j)}(x)$ stands for the Hankel functions, $H_n^{(1)\prime}(x) = \frac{d}{dx} H_n^{(1)}(x)$, $\rho_< = \min(\rho, \rho_1)$, $\rho_> = \max(\rho, \rho_1)$. Let us denote the direct and inverse Fourier transform operator as

$$\begin{aligned} W_\varphi[a_n] &= A(\varphi) = \sum_{n=-\infty}^{\infty} a_n e^{in\varphi}, \\ W_n^{-1}[A(\varphi)] &= a_n = \frac{1}{2\pi} \int_{-\pi}^{\pi} A(\varphi) e^{-in\varphi} d\varphi. \end{aligned}$$

By using boundary condition b) in (2) and applying the operator W_n^{-1} to Equation (4) for $\rho = b - \beta$ $(0 < \beta \ll 1)$, upon proceeding to the limit $\beta \to 0$ and accounting for the well-known relation for the Hankel functions $H_{-n}^{(j)}(x) = (-1)^n H_n^{(j)}(x)$, we obtain the following finite-difference equation [16]

$$u_n = -\eta_2^{-1} s_n u_{n-1} + g_n, \quad (-\infty < n < \infty), \tag{8}$$

where

$$u_n = W_n^{-1}[U(b,\varphi)],\ s_n = \frac{H_{n,1}^{(11)(10)}(x,y)}{H_{n,\delta}^{(11)(10)}(x,y)}, \tag{9}$$

$$g_n = -\frac{I^{(m)} e^{-in\varphi_0}}{2\pi i \eta_2 k y} \frac{H_n^{(10)}(x, k\rho_0)}{H_{n,\delta}^{(11)(10)}(x,y)},$$

$$H_{n,\delta}^{(11)(10)}(x,y) = H_n^{(11)}(x,y) - i\eta_0 \delta H_n^{(10)}(x,y),$$

$$H_{n,1}^{(11)(10)}(x,y) = H_{n,\delta}^{(11)(10)}(x,y)|_{\delta=1},\ x = ka,\ y = kb,\ \delta = \eta_1/\eta_2, .$$

The solution of (8) is constructed basing of the factorization of its coefficient (see Appendix). From relationships (4, 5, 6, 9, A2, A4), upon rather cumbersome transformations, we get the following expression for the Hertz potential

$$U(\vec{\rho}, \vec{\rho_0}) = \frac{I^{(m)}}{8k}(U_r(\vec{\rho}, \vec{\rho_0}) + U_{ir}(\vec{\rho}, \vec{\rho_0})), \tag{10}$$

where the regular part with a simple angular dependence as $\varphi - \varphi_0$ is

$$U_r(\vec{\rho}, \vec{\rho_0}) = \sum_{n=-\infty}^{\infty} e^{in(\varphi-\varphi_0)} \frac{H_n^{(10)}(x, k\rho_<^0)}{H_{n,\alpha}^{(11)(10)}(x,y)} H_{n,\alpha}^{(10)(00)}(y, k\rho_>^0), \tag{11}$$

$$\alpha = \begin{cases} 1 & \text{for } |\eta_2| < 1 \\ \delta & \text{for } |\eta_2| > 1, \end{cases}$$

$\rho_<^0 = \min(\rho, \rho_0)$, $\rho_>^0 = \max(\rho, \rho_0)$, while the irregular part is

$$U_{ir}(\vec{\rho}, \vec{\rho_0}) = -4\frac{\eta_0(1-\delta)}{\pi y} \sum_{n=-\infty}^{\infty} e^{in(\varphi-\varphi_0)} \frac{H_n^{(10)}(x, k\rho)}{H_{n,1}^{(11)(10)}(x,y)} U_n(\vec{\rho_0}), \tag{12}$$

$$U_n(\vec{\rho_0}) = \sum_{m=1}^{\infty} e^{-im\varphi_0}(-\eta_2)^m \prod_{j=1}^{m} \frac{H_{n+j,\,\delta}^{(11)(10)}(x,y)}{H_{n+j,\,1}^{(11)(10)}(x,y)} \frac{H_{n+m}^{(10)}(x,k\rho_0)}{H_{n+m,\,\delta}^{(11)(10)}(x,y)}, \quad \text{for } |\eta_2| < 1, \tag{13}$$

$$U_n(\vec{\rho_0}) = -\sum_{m=1}^{\infty} e^{im\varphi_0}(-\eta_2)^{-m} \prod_{j=0}^{m-1} \frac{H_{n-j,\,1}^{(11)(10)}(x,y)}{H_{n-j,\,\delta}^{(11)(10)}(x,y)} \frac{H_{n-m}^{(10)}(x,k\rho_0)}{H_{n-m,\,\delta}^{(11)(10)}(x,y)}, \quad \text{for } |\eta_2| > 1. \tag{14}$$

The first term in (10) coincides with the solution to the problem where the source in question excites the regular coaxial waveguide whose reduced surface impedance of the wall $\rho = b$ equals $\eta_0\alpha$. In order to make certain that function (10) is really the desired solution, substitute (10) directly into (1) and (2).

3. WATSON TRANSFORMATION

The series in n in (11), (12) represent expansions in terms of *radially* propagating waves. Since the number of the terms contributing significantly to the field are of the order of $O(ka)$ (see [17]), Equation (10) is convenient for analysis only for $ka \ll 1$. For the applications considered in the present paper, the range $ka \gg 1$ is important, where expansions in terms of *azimuthally* propagating 'creeping' waves (alternative to the series in (11), (12)) obtainable from (10) by Watson transformations [15, 17, 18] are rapidly convergent. Without going into details we give the result of this transformation:

$$U_r(\vec{\rho},\vec{\rho_0}) = -2\pi \sum_{s=1}^{\infty} \frac{H_{\nu_s}^{(10)}(x,k\rho_<^0)}{\sin\pi\nu_s \dot{H}_{\nu_s,\,\alpha}^{(11)(10)}(x,y)} \times H_{\nu_s,\,\alpha}^{(10)(00)}(y,k\rho_>^0)\cos(\pi-\Delta\varphi)\nu_s, \tag{15}$$

$$U_{ir}(\vec{\rho},\vec{\rho_0}) = 4i\frac{\eta_0^2(1-\delta)^2}{y} \sum_{s=1}^{\infty} \frac{H_{\nu_s}^{(10)}(x,y)}{\sin\pi\nu_s \dot{H}_{\nu_s,\,\alpha}^{(11)(10)}(x,y)} \times\Big(U(\vec{\rho},\vec{\rho_0};\nu_s)e^{i(\Delta\varphi-\pi)\nu_s} + U(\vec{\rho},\vec{\rho_0};-\nu_s)e^{-i(\Delta\varphi-\pi)\nu_s}\Big), \tag{16}$$

where $\dot{H}_{\nu_s,\,\alpha}^{(11)(10)}(x,y) = \frac{\partial}{\partial\nu} H_{\nu,\,\alpha}^{(11)(10)}(x,y)\big|_{\nu=\nu_s}$; $\Delta\varphi = \varphi - \varphi_0 > 0$, ν_s are the roots of the equation

$$H_{\nu,\,\alpha}^{(11)(10)}(x,y) = 0, \tag{17}$$

$$U(\vec{\rho},\vec{\rho_0};\nu_s) = \sum_{m=1}^{\infty} e^{-im\varphi_0}(-\eta_2)^m \sum_{l=0}^{m} e^{-il\Delta\varphi}\Pi_m^{(l)}(\nu_s - l) \times \frac{H^{(10)}_{\nu_s-l}(x,k\rho)}{H^{(11)(10)}_{\nu_s-l,\,\delta}(x,y)} \frac{H^{(10)}_{\nu_s-l+m}(x,k\rho_0)}{H^{(11)(10)}_{\nu_s-l+m,\,\delta}(x,y)}, \quad \text{for } |\eta_2|<1, \tag{18}$$

$$U(\vec{\rho},\vec{\rho_0};\nu_s) = \sum_{m=1}^{\infty} e^{im\varphi_0}(-\eta_2)^{-m} \sum_{l=0}^{m} e^{il\Delta\varphi}\tilde{\Pi}_m^{(l)}(\nu_s + l) \times \frac{H^{(10)}_{\nu_s+l}(x,k\rho)}{H^{(11)(10)}_{\nu_s+l,\,1}(x,y)} \frac{H^{(10)}_{\nu_s+l-m}(x,k\rho_0)}{H^{(11)(10)}_{\nu_s+l-m,\,1}(x,y)}, \quad \text{for } |\eta_2|>1, \tag{19}$$

$$\Pi_m^{(l)}(\nu) = \prod_{j=0,\,j\neq l}^{m} \frac{H^{(11)(10)}_{\nu+j,\,\delta}(x,y)}{H^{(11)(10)}_{\nu+j,\,1}(x,y)}, \quad \tilde{\Pi}_m^{(l)}(\nu) = \prod_{j=0,\,j\neq l}^{m} \frac{H^{(11)(10)}_{\nu-j,\,1}(x,y)}{H^{(11)(10)}_{\nu-j,\,\delta}(x,y)}. \tag{20}$$

It can be shown following the methodology given in [19] that the roots of Equation (17) are located symmetrically in the first and the third quadrants of the ν-plane. In the analysis which follows, we restrict ourselves to the case of ($|\eta_2| < 1$). The CS phenomenon has been detected on the waves coming to the receiver along the shortest route. Therefore, extracting them from (15), (16) and placing the receiver and the source onto the boundary $\rho = a$ at the points with angular coordinates φ and φ_0 respectively, we arrive at the following expression for the Hertz vector

$$\frac{4k}{I^{(m)}} U(\vec{\rho},\vec{\rho_0})\big|_{\rho=\rho_0=a} = -\frac{4}{x}\sum_{s=1}^{\infty} \frac{e^{i\Delta\varphi\nu_s}}{\dot{H}^{(11)(10)}_{\nu_s,\,1}(x,y)} V_s(\varphi,\varphi_0), \tag{21}$$

$$V_s(\varphi,\varphi_0) = V_r(\nu_s) + V_{ir}(\varphi,\varphi_0;\nu_s), V_r(\nu_s) = H^{(10)(00)}_{\nu_s,\,1}(y,x), \tag{22}$$

$$V_{ir}(\varphi,\varphi_0;\nu_s) = -16\frac{i\eta_0(1-\delta)}{\pi^2 xy}\big\{u_s^+(\varphi_0) + [1 + i\eta_0(1-\delta) \times H^{(10)}_{\nu_s}(x,y)u_s^+(\varphi_0)]u_s^-(\varphi)\big\}, \tag{23}$$

$$u_s^{\pm}(\varphi) = \sum_{m=1}^{\infty} \frac{e^{-im\varphi}(-\eta_2)^m}{H^{(11)(10)}_{\nu_s\pm m,\,\delta}(x,y)} \prod_{j=l}^{m} \frac{H^{(11)(10)}_{\nu_s\pm j,\,\delta}(x,y)}{H^{(11)(10)}_{\nu_s\pm j,\,1}(x,y)}. \tag{24}$$

To simulate the CS phenomenon let us fix the angular distance $\Delta\varphi$ between the receiver and the source. In this case, the function

$$\tilde{U}(\varphi) = \frac{4k}{I^{(m)}} U(\vec{\rho},\vec{\rho_0})\big|_{\rho=\rho_0=a,\,\varphi_0=\varphi-\Delta\varphi}, \ (0 \le \varphi \le 2\pi), \tag{25}$$

may be considered as the 'diurnal dependence' of the received signal. To ensure a nonzero diurnal phase change, the curve $V_s(\varphi, \varphi_0)$ in the complex plane must enclose the origin of coordinates. Since the regular term V_r in (22) does not depend on φ, while the irregular term V_{ir} for $\varphi_0 = \varphi - \Delta\varphi$ is proportional to $e^{-i\varphi}$, then the following inequality is the necessary condition for the occurrence of CS in the model considered:

$$|V_r(\nu_s)| < |V_{ir}(\varphi, \varphi_0; \nu_s)|. \tag{26}$$

4. NUMERICAL EXPERIMENT

Let us calculate the Hertz potential $\tilde{U}(\varphi)$ from (21)–(25) for the frequency $f = 10\,\text{KHz}$ and waveguide dimensions $a = 6370\,\text{km}$ and $b - a = 60\,\text{km}$. Since $ka = 1335.06 \gg 1$, we will use the Olver uniform asymptotic representation [20] to calculate the Hankel functions $H_\nu^{(j)}(x)$ along with their derivatives with respect to argument and index. The roots of transcendental Equation (17) for $\alpha = 1$ can be determined by the Newton-Raphson method [21]. Location of several first roots as a function of complex parameter η_0 has been analyzed. Fig. 2 illustrates typical trajectories of the first two roots ν_s ($s = 1, 2$) in the complex ν-plane for several fixed values of $\arg \eta_0$ as $|\eta_0|$ increases. The real values ν_1^0 and ν_2^0 correspond to zero impedance. The sign '+' indicates the degenerate value $\nu_{12}^{deg} \approx 1324.91 + 21.64i$ of these two roots corresponding to the impedance $\eta_{12}^{deg} \approx 0.1826 - 0.1127i$ (see [13, 22]). It is easily seen that an abrupt change in the behavior of the eigenvalues of waveguide modes occurs when crossing the ray $\arg \eta_0 = \arg \eta_{12}^{deg} \approx 58.31°$.

Let us consider first the case of weakly irregular waveguides $\delta \approx 1$. Then for $|\eta_2| \ll 1$ we have from (23)

$$V_{ir}(\varphi, \varphi_0; \nu_s) = (\eta_1 - \eta_2) V_{ir}^0(\varphi, \varphi_0; \nu_s), \tag{27}$$

$$V_{ir}^0(\varphi, \varphi_0; \nu_s) = -\frac{16 i \eta_0}{\pi^2 x y} e^{-i\varphi_0} \left[\frac{1}{H_{\nu_s+1,1}^{(11)(10)}(x, y)} + \frac{e^{-i\Delta\varphi}}{H_{\nu_s-1,1}^{(11)(10)}(x, y)} \right] + O(1 - \delta). \tag{28}$$

In Fig. 3, the level curves of the function $|V_{ir}^0(\varphi, \varphi_0; \nu)|$ for $\varphi_0 = \varphi - \Delta\varphi$ are shown in the complex ν-plane for the most interesting domain of variation of the eigenvalues of the first and the second modes for the impedance $i\eta_0 = H_\nu^{(11)}(x, y)/H_\nu^{(10)}(x, y)$ satisfying Equation (17). The angular distance between the receiver

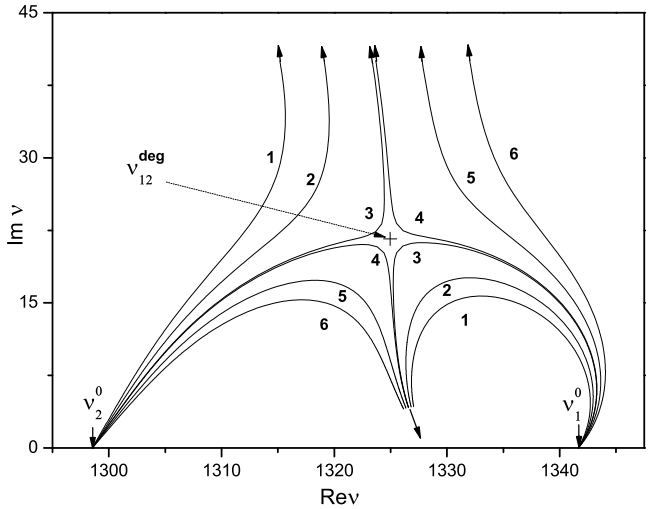

Figure 2. Trajectories of the first two roots ν_1, ν_2 of Equation (17) in the complex ν-plane for several fixed values of $\arg \eta_0$ as $|\eta_0|$ increases ($0 \leq |\eta_0| \leq 0.5$); $\arg(i\eta_0)$ equal to (1) 63.43°, (2) 60.94°, (3) 58.39°, (4) 58.21°, (5) 55.83°, (6) 53.37°.

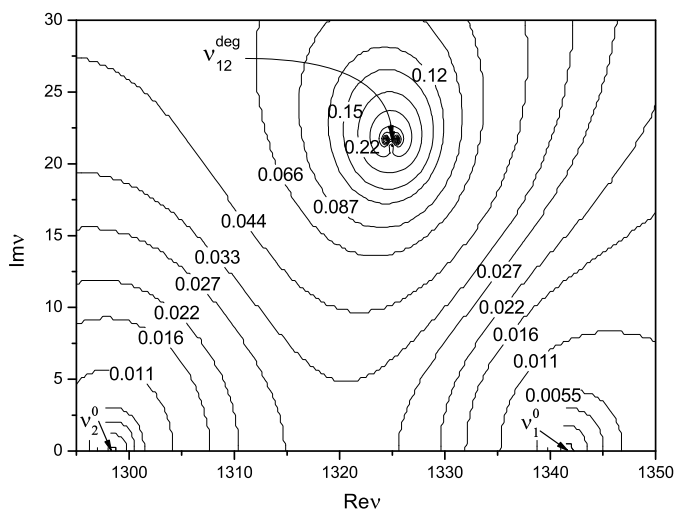

Figure 3. The level curves of the function $|V_{ir}^0(\varphi_0 + \Delta\varphi, \varphi_0; \nu)|$ for $\Delta\varphi = 2$, ($\max_\nu |V_{ir}^0(\varphi_0 + 2, \varphi_0; \nu)| = 3.0517$, $\nu_{\max} = 1325.5 + 21.75i$, $|V_{ir}^0(\varphi_0+2, \varphi_0; \nu_1^0)| = 1.2593 \cdot 10^{-4}$, $|V_{ir}^0(\varphi_0+2, \varphi_0; \nu_2^0)| = 4.5397 \cdot 10^{-5}$).

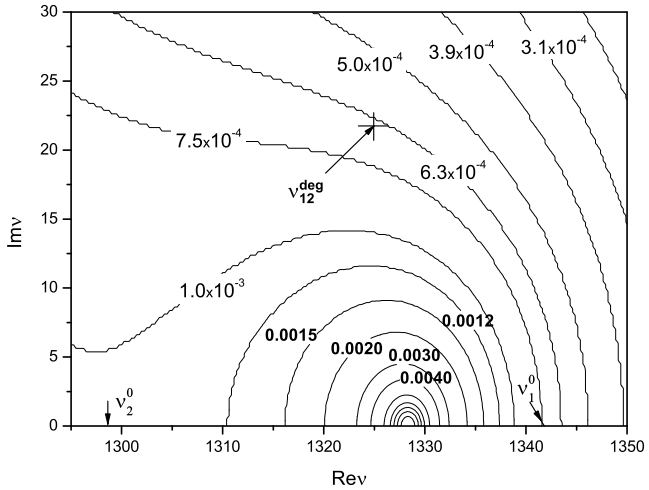

Figure 4. The level curves of the function $|V_r(\nu)|$, ($\max_\nu |V_r(\nu)| = 0.1561$, $\nu_{\max} = 1328.25$).

and the transmitter is $\Delta\varphi = 2$, therefore, as it follows from numerical estimations, the contribution of the third and higher modes can be neglected. Minimal values of $|V_{ir}^0(\varphi, \varphi_0; \nu)|$ are located in the vicinity of the points ν_1^0 and ν_2^0, while the maximum is close to ν_{12}^{deg}. By comparing these results with the level curves of $|V_r(\nu)|$ from Fig. 4, we arrive at the conclusion that for small η_0, for which $r_{imp} \ll 1$ and $\nu_{1,2}$ tends to $\nu_{1,2}^0$, the inequality $|V_r(\nu)| > |V_{ir}^0(\varphi, \varphi_0; \nu)|$ holds, and hence, CS is impossible in view of (26), (27). Let η_0 be growing and approaching η_{12}^{deg}. At the same time, r_{imp} increases, the center of the impedance circle η_{imp} tends to η_{12}^{deg}, while the eigenvalues of the first and second modes approach the point ν_{12}^{deg}, in the vicinity of which an amplitude of the irregular part of $|V_{ir}^0(\varphi, \varphi_0; \nu)|$ is maximal. Then for not-too-small values of $|\eta_1 - \eta_2|$ inequality (26) holds. In other words, it follows from the foregoing numerical estimates for the functions $|V_r(\nu)|$ and $|V_{ir}^0(\varphi, \varphi_0; \nu)|$ for weakly irregular waveguides that there exists a *threshold value* of the hodograph radius r_{imp}^{cs} of the impedance $\eta(\varphi)$ (3) such that the CS phenomenon is impossible for $r_{imp} < r_{imp}^{cs}$, while for $r_{imp} > r_{imp}^{cs}$ it occurs at least for the hodographs located in the vicinity of η_{12}^{deg}. As an angular distance $\Delta\varphi$ increases, the probability that the phenomenon in question will occur is growing too, all factors being equal. A similar situation holds when a degree of waveguide irregularity grows, i.e., with increasing r_{imp}.

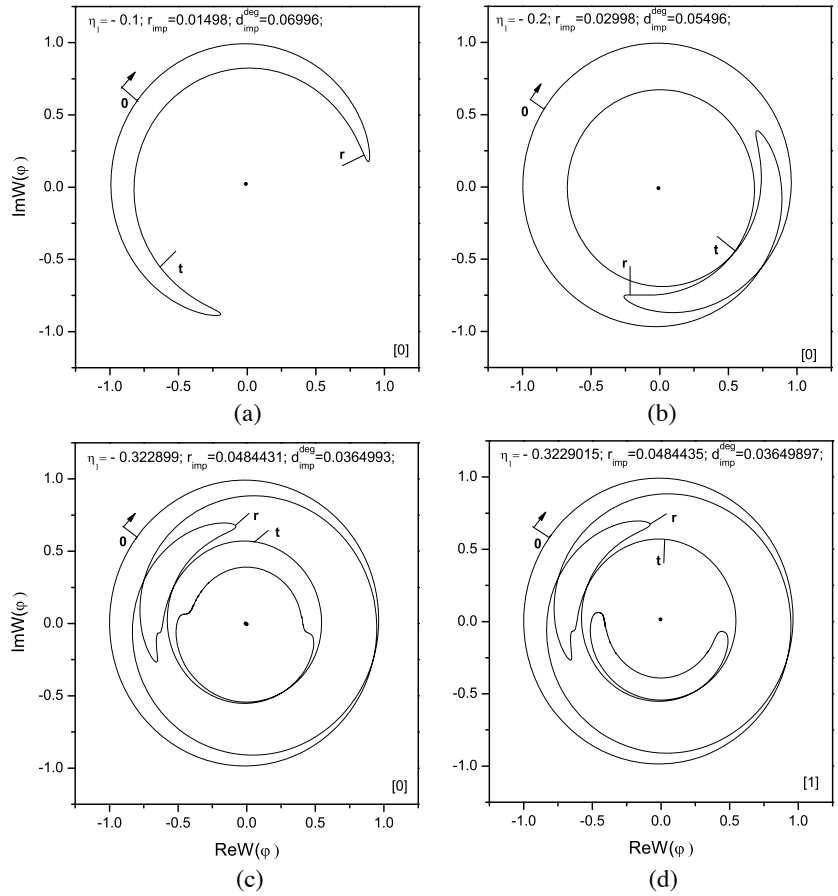

Figure 5. The normalized value of 'diurnal record' of the received signal $W(\varphi)$, ($\eta_0 = 0.1455 - 0.03638i$, $\eta_2 = 0.0001$, $\Delta\varphi = 2$).

Figures 5 and 6 present the results of the simulation of '*diurnal record*' of the received signal or, in other words, the φ-dependencies of the normalized value

$$W(\varphi) = \left(\lg\left(\max_{0\le\varphi\le 2\pi} |\tilde{U}(\varphi)|\right)\tilde{U}(\varphi)\right) / \left(\lg\left(|\tilde{U}(\varphi)|\right)|\tilde{U}(\varphi)|\right),$$

for $\Delta\varphi \le \varphi \le 2\pi + \Delta\varphi$ and the fixed angular distance $\Delta\varphi = 2$ between the source and the receiver. On these curves three following values of the received signal are marked: '0' corresponds to the initial moment of the record ($\varphi_0 = 0, \varphi = \Delta\varphi$), '$r$'('$t$') corresponds to the moment of time when the receiver (the transmitter) is passing through the waveguide

cross-section $\varphi = \varphi_{cr}$, where the surface impedance value is most close to η_{12}^{deg} (see Fig.7). The number of lost phase cycles are shown in these figures in square brackets $[m]$; d_{imp}^{deg} is the distance from the impedance circle to the point η_{12}^{deg}. The numerical experiment has shown that the CS phenomenon is nonexistent for hodographs of the impedance $\eta(\varphi)$ remote from the segment $l_{cs} = \{0 < |\eta| \leq \eta_{12}^{deg},\ \arg\eta = \arg\eta_{12}^{deg}\}$ (Figs. 5(a), (b), (c)). As r_{imp} increases, $W(\varphi)$ behavior becomes more complex; when the circle $\eta(\varphi)$ intersects l_{cs}, CS occurs (Fig. 5(d)) for $r_{imp} \approx 0.04844$. At the same time, the signal amplitude decreases over small variation interval (of the order of $0.01°$) of φ. As r_{imp} grows,

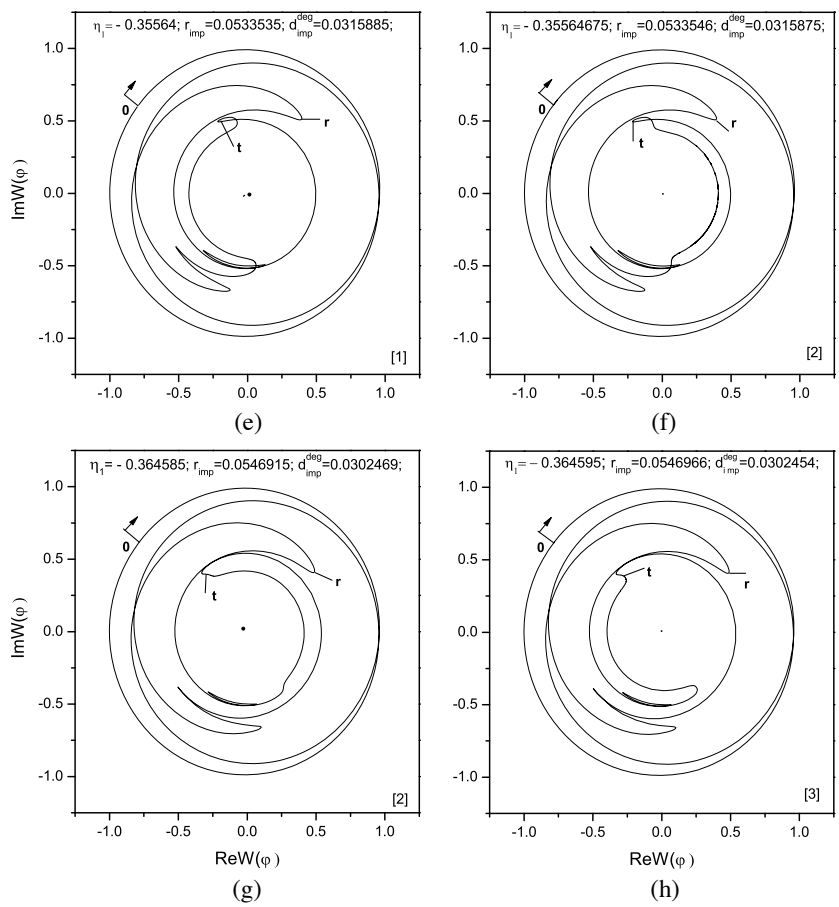

Figure 6. The normalized value of 'diurnal record' of the received signal $W(\varphi)$, ($\eta_0 = 0.1455 - 0.03638i$, $\eta_2 = 0.0001$, $\Delta\varphi = 2$).

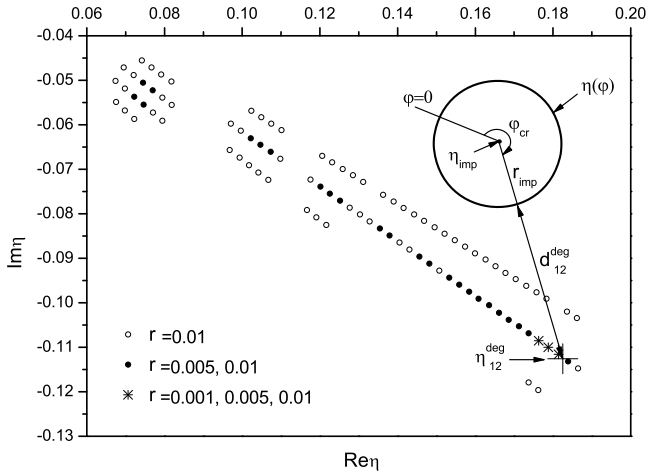

Figure 7. The domains in the complex η-plane, for which the CS phenomenon takes place at the given radius r_{imp} and angle $\Delta\varphi = 2$.

at $r_{imp} \approx 0.05335$ (Fig. 6(f)), the CS phenomenon for two cycles, at $r_{imp} \approx 0.05469$ (Fig. 6(h)) for three cycles, and so forth is observable. A similar situation holds for the circle $\eta(\varphi)$, whose center is located in the vicinity of l_{cs}; however, the CS begins for lesser values of r_{imp}. Each CS phenomenon is accompanied by a sharp decrease in the signal amplitude, what is typical for the CS in a natural waveguide [6, 9]. The part played by the segment l_{cs} in the initiation of the CS phenomenon within the limits of the given model can be explained as follows: for the impedances only in the vicinity of this segment, the eigenvalues ν_1 and ν_2 have closely spaced imaginary parts, and consequently, amplitudes of the first and the second modes are nearly equal. In addition, when η_0 is moving along l_{cs} towards the point η_{12}^{deg}, the real parts of ν_1 and ν_2 come close together (curves 3 or 4 in Fig. 2), and consequently, the phase velocities of these modes approach each other.

Of some interest is a localization of the domains in the complex η-plane, for which the CS phenomenon takes place at the given radius r_{imp} and angle $\Delta\varphi$. It is seen from Fig. 7 (Dots indicate center positions for hodographs of radiuses 0.001, 0.005 and 0.01, for which CS occurs at $\Delta\varphi = 2$.) that with increasing r_{imp} the CS phenomenon develops initially in the immediate vicinity of the point η_{12}^{deg}, and then, as r_{imp} grows, this area is extending occupying a constantly increasing part of the segment l_{cs}. For hodographs with fixed centers, the CS phenomenon having developed at some r_{imp}, persists for larger values of the radius.

5. CONCLUSION

A model of the ring waveguide of a fixed cross-section whose irregularity is caused only by the behavior of the surface impedance distribution of its wall has been proposed. Hence we have excluded from consideration the diffraction effect of wave transformation on a spatial inhomogeneity of the wall; only the mode degeneracy effect being inherent in waveguides with finite absorption is analyzed. For a class of circular hodographs of surface impedance the analytical solution of the corresponding boundary-value problem is obtained. The results of the numerical experiment for widely separated ($1 \leq \Delta\varphi \leq \pi$) transmitter and receiver have shown that the CS phenomenon here is directly related to the degeneracy of the first and the second modes. It is threshold in character and occurs in the waveguides with sufficiently high irregularity of walls whose impedance is distributed in the neighborhood of the degenerate value η_{12}^{deg}. Having developed this phenomenon persists as the radius of the impedance hodograph (a degree of waveguide irregularity) increases. At the same time, the domain of the impedance complex plane where CS takes place is extending occupying a constantly increasing part of the segment joining the origin of coordinates and the point η_{12}^{deg}.

It has been demonstrated with a waveguide of a fixed cross-section that the CS phenomenon in irregular lossy waveguides (in particular, in the earth-ionosphere waveguide) may be caused by the interconversion of two dominant waveguide modes in the neighborhood of their degeneracy regime rather than by the diffraction effect of rescattering of the principal mode into the higher modes on a spatial inhomogeneity of the waveguide wall, as it is customary to assume.

APPENDIX A. THE SOLUTION OF THE FINITE-DIFFERENCE EQUATION (8)

The solution of (8) is constructed basing of the following factorization of its coefficient:

$$s_n = \frac{\sigma_n}{\sigma_{n-1}^{\gamma}}, \tag{A1}$$

where $\gamma > 1$ is an auxiliary parameter. Taking the logarithm of (A1) and applying the operators W and W^{-1}, we can easily show that

$$\ln \sigma_n = W_n^{-1}\left[W_\theta\left[\ln s_n\right] / \left(1 - \gamma e^{i\theta}\right)\right] = -\gamma^n \sum_{m=n+1}^{\infty} \ln s_m \gamma^{-m}$$

whence it follows that for $\gamma = 1$ we have

$$\sigma_n = \begin{cases} \prod_n^{m=0} s_m & \text{for } n \geq 0, \\ 1 & \text{for } n = -1, \\ \prod_{n+1}^{m=-1} s_m^{-1} & \text{for } n \leq -2. \end{cases} \tag{A2}$$

By substituting (A1) with $\gamma = 1$ into Equation (8), we arrive at the equation

$$\frac{u_n}{\sigma_n} = -\eta_2^{-1} \frac{u_{n-1}}{\sigma_{n-1}} + \frac{g_n}{\sigma_n}, \ (-\infty < n < \infty). \tag{A3}$$

The solution of this equation is similar to that of the equation for $\ln \sigma_n$, which can be derived by taking the logarithm of (A1), and is as follows

$$\frac{u_n}{\sigma_n} = W_n^{-1} \left[W_\theta \left[g_n / \sigma_n \right] / \left(1 + \eta_2^{-1} e^{i\theta} \right) \right]. \tag{A4}$$

REFERENCES

1. Johler, J. R. and L. A. Berry, *Propagation Radio Waves at Frequencies Below 300 kc/s*, Pergamon Press, Oxford, Paris, 1964.
2. Alpert, Ya. L., E. G. Guseva, and D. S. Fligel, *Propagation of Low-frequency Electromagnetic Waves in the Earth-ionosphere Waveguide*, Nauka, Moscow, 1967 (in Russian).
3. Makarov, G. I., V. V. Novikov, and A. B. Orlov, "The current status of research on the VLF propagation in the earth-ionosphere waveguide," *Izv. Vuzov. Radiofizika*, Vol. 13, No. 3, 321–355, 1970 (in Russian).
4. Simpson, J. J. and A. Taflove, "A review of progress in FDTD Maxwell's equations modeling of impulsive subionospheric propagation below 300 KHz," *IEEE Trans. Antennas Propag.*, Vol. 55, No. 6, 1582–1590, 2007.
5. Lynn, K. W., "Multisite observations of the VLF transequatorial propagation anomaly," *Radio Science*, Vol. 4, No. 3, 203–212, 1969.
6. Walker, D., "Phase steps and amplitude fading of VLF signals at dawn and dusk," *Radio Science*, Vol. 69D, No. 11, 1435–1443, 1965.
7. Bahar, E. and J. R. Wait, "Propagation in a model terrestrial waveguide of nonuniform height: Theory and experiment," *Radio Science*, Vol. 69D, No. 11, 1445–1463, 1965.
8. Wait, J. R., "Mode conversion and refraction effects in the earth-ionosphere waveguide for VLF radio waves," *Journal of Geophysical Research*, Vol. 73, No. 11, 3537–3548, 1968.

9. Katsenelenbaum, B. Z., *The Theory of Irregular Waveguides with Slowly Varying Parameters*, Academy of Science Press, Moscow, 1961 (in Russian).
10. Bolotovskii, Ya. E. and G. I. Makarov, "Intersection of VLF-signal path and the 'day-night' boundary," *Problems of Diffraction and Wave Propagation*, No. 11, 142–158, Leningrad State University Press, Leningrad, 1972 (in Russian).
11. Pappert, R. A. and J. A. Ferguson, "VLF/LF mode conversion model calculations for air to air transmissions in the earth-ionosphere waveguide," *Radio Science*, Vol. 21, No. 4, 551–558, 1986.
12. Budden, K. G., "The critical coupling of modes in a tapered earth-ionosphere wave guide," *Math. Proc. Camb. Phil. Soc.*, Vol. 77, 567–580, 1975.
13. Krasnushkin, P. Ye. and Ye. N. Fedorov, "About multiplicity of wave numbers of normal modes in stratified media," *Radiotekhnika i Elektronika*, Vol. 17, No. 6, 1129–1140, 1972 (in Russian).
14. Westerlund, S. and F. H. Reder, "VLF radio signal propagating over the Greenland ice-sheet," *JATP*, Vol. 35, No. 8, 1973.
15. Tyras, G., *Radiation and Propagation of Electromagnetic Waves*, Academic Press, New York and London, 1969.
16. Gakhov, F. D. and Yu. I. Cherskii, *Convolution Equations*, Nauka, Moscow, 1978 (in Russian).
17. Makarov, G. I., V. V. Novikov, and S. T. Rybachek, *Radiowave Propagation in the Earth-ionosphere Waveguide and in the Ionosphere*, Nauka, Moscow, 1994 (in Russian).
18. Felsen, L. B. and N. Marcuvitz, *Radiation and Scattering of Waves*, Prentice-Hall, Englewood Cliffs, NJ, 1973.
19. Keller, J. B., S. I. Rubinow, and M. Goldstein, "Zeros of Hankel functions and poles of scattering amplitudes," *Journal of Mathematical Physics*, Vol. 4, No. 6, 829–832, 1963.
20. Paknys, R., "Evaluation of Hancel functions with complex argument and complex order," *IEEE Trans. Antennas Propag.*, Vol. 40, No. 5, 569–578, 1992.
21. Tian, Y. B. and J. Qian, "Ultraconveniently finding multiple solutions of complex transcendental equations based on genetic algorithm," *Journal of Electromagnetic Waves and Applications*, Vol. 20, No. 4, 475–488, 2006.
22. Hanson, G. W. and A. B. Yakovlev, "Investigation of mode interaction on planar dielectric waveguides with loss and gain," *Radio Science*, Vol. 34, No. 6, 1349–1359, Nov.–Dec. 1999.